High-spin γ-ray spectroscopy in $Z=83$ isotopes: ^{199,201}Bi

W. F. Piel, Jr., T. Chapuran,* K. Dybdal,† D. B. Fossan, and T. Lönnroth‡

Department of Physics, State University of New York at Stony Brook, Stony Brook, New York 11794

D. Horn§ and E. K. Warburton

Department of Physics, Brookhaven National Laboratory, Upton, New York 11973

The properties of high-spin states in ^{199,201}Bi have been studied with the ^{194,196}Pt(^{10}B,5nγ)^{199,201}Bi reactions at energies between 57 and 72 MeV. In-beam measurements of γ-ray excitations, γ-γ-t coincidences and correlations, γ-ray angular distributions, and pulsed-beam-γ timing were performed with Ge detectors to determine level energies, decay schemes, γ-ray multipolarities, J^π assignments, and isomeric lifetimes. Levels along and near the yrast lines were established up to $J \approx \frac{33}{2}$, including a number of isomers. The systematic trends of three-quasiparticle level energies in odd-mass Bi isotopes have been extended and compared with calculations involving neutron-hole configurations of the Pb-core isotones. The transition strengths extracted for ^{199,201}Bi are compared to Pb-region values. In addition, an isomeric lifetime was measured in ^{200}Bi.

I. INTRODUCTION

Nuclei in the vicinity of the doubly-closed nucleus ^{208}Pb ($Z=82,N=126$) have been successfully interpreted in terms of shell-model configurations of a few valence nucleons coupled to a core in its 0^+ ground state. High-spin yrast states are particularly suited for detailed structure studies, since they usually are dominated by a unique wave-function component. Recently the isotopic chains of odd-A bismuth ($Z=83$) and astatine ($Z=85$) have been studied for $N<126$ in great deal with (HI,xn) reactions and in beam γ-ray and conversion electron spectroscopy. For the astatine nuclei,[1-4] the studies have reached ^{201}At($\pi^3 \nu^{-10}$) and for bismuth,[5-9] ^{203}Bi($\pi\nu^{-6}$). The motivation for pursuing these studies as a function of neutron number stems from the competition that is expected to develop at large neutron deficiencies between the quasiparticle and collective degrees of freedom.

There are two aims in these studies. The first is to examine the quasiparticle behavior of the well-known proton states, defined in the $N=126$ isotones ^{209}Bi(π) and ^{211}At(π^3), when coupled to neutron-hole states in the even-A lead cores. The assignment of specific configurations, where mixing is not strong, is important in order to interpret excitation energies and interaction strengths. The second aim is to search, as the $N=126$ neutron shell is increasingly depleted, for the onset of collectivity as manifested by, e.g., enhanced $B(E2)$ transitions and a participation of collective structures in the yrast spectra. In the $Z > 50$ transition region, by comparison, the $g_{9/2}$ proton-hole intruder states induce low-lying $\Delta J = 1$ collective bands, which coexist with the quasiparticle states, in the odd-A isotopes of Sb ($Z=51$),[10] I ($Z=53$),[11] and CS ($Z=55$).[12] The $h_{11/2}$ proton hole, which would be the corresponding high-spin intruder for the $Z > 82$ transition region, is expected to drop in energy with increasing neutron deficiency for the odd-A Bi ($Z=83$) nuclei as does the $s_{1/2}$ proton hole.[13] Such collective phenomena serve

as probes of the potential energy surfaces under the changing stress of large imbalances in the number of neutrons and protons.

In the present paper, the high-spin states in ^{201}Bi ($N=118$) and ^{199}Bi ($N=116$) have been studied via the (^{10}B,5n) reaction. Their interpretation is simplified since the structure of the underlying core nuclei ^{200,198}Pb are known in some detail.[14] Extended studies into ^{197}Bi ($N=114$) and ^{195}Bi ($N=112$) are being reported in subsequent papers.[15,16] When the present study began, only scant data on high-spin states in ^{201,199}Bi were available. Beta-decay studies[17] of the $\frac{13}{2}^+$ isomers in ^{201,199}Po had revealed several excited states in ^{201,199}Bi, although these results had been questioned because of errors found[5] in the same study for ^{203}Bi. Some information on low-spin states was known.[13,18] Preliminary reports of the present work have been presented.[19] Recently, information on the level scheme of ^{201}Bi has been obtained by the (α,6n) reaction during a study of neighboring ^{202}Bi.[20]

The experimental techniques used in the present (HI,$xn\gamma$) study are briefly outlined in Sec. II. In Sec. III, the experimental results are presented and a discussion of the interpretations is given in Sec. IV.

II. EXPERIMENTAL TECHNIQUES

High-spin states of ^{199,201}Bi were studied via the ^{194,196}Pt(^{10}B,5nγ)^{199,201}Bi reactions with ^{10}B beams of 57—72 MeV from the Brookhaven National Laboratory tandem Van de Graaff facility. The ^{194}Pt target (enriched to $>95\%$) was 7 mg/cm^2 thick ($\Delta E = 4.2$ MeV), while the ^{196}Pt target (enriched to $>95\%$) was 3.6 mg/cm^2 ($\Delta E = 2.2$ MeV). The γ rays produced were detected with Ge(Li) detectors having energy resolutions of 1.8—2.3 keV full width at half maximum (FWHM) and efficiencies of 10—20% (relative to a 7.6 cm $\times$7.6 cm NaI detector at 1.33 MeV). In addition, a 7 mm thick intrinsic-Ge planar detector was used for part of the measurements to detect

the lower energy photons (50—150 keV) with higher resolution and less compton background.

Gamma-ray excitation functions were recorded from 57 to 72 MeV for the ^{196}Pt target to determine the optimum beam energy and to identify transitions in ^{201}Bi. The γ-ray yields were measured relative to the integrated beam current as a function of bombarding energy. The optimum beam energy was found empirically to be 67 MeV for the ^{196}Pt target; using this result, the optimum energy to study ^{199}Bi was estimated to be 70 MeV for the ^{194}Pt target. An inspection of the γ-ray singles spectrum produced by 70 MeV ^{10}B + ^{194}Pt, which showed weak but comparable populations of the ^{198}Bi and ^{200}Bi odd-odd channels, indicated that this energy was indeed suitable for the ^{199}Bi experiments.

In order to obtain information on the transition multipolarities, the γ-ray angular distributions were measured in singles at seven angles between 75° and 160° relative to the beam direction with a second detector at $-90°$ serving as a monitor. Angular-distribution coefficients A_2/A_0 and A_4/A_0 as well as the relative γ-ray intensities I_γ were extracted from least-squares fits to the normalized photopeak areas; a small solid angle correction was applied.

Gamma-γ coincidence measurements were performed at the optimum beam energies with two Ge(Li) detectors
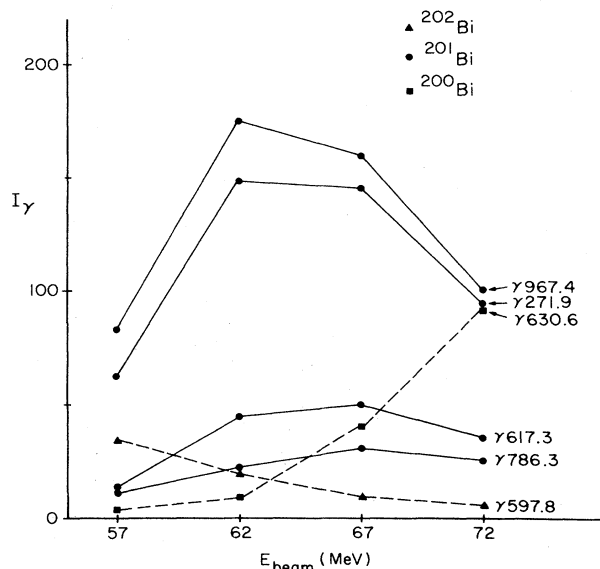

FIG. 1. Relative ^{200,201,202}Bi γ-ray photopeak intensities recorded at $\theta = 54.7°$ produced by ^{10}B + ^{196}Pt and corrected for the efficiency of the Ge(Li) detector. The γ-ray energies are listed in keV. The statistical uncertainty for each datum is smaller than the symbol used. The average beam energy loss in traversing the target is 2.6 MeV.
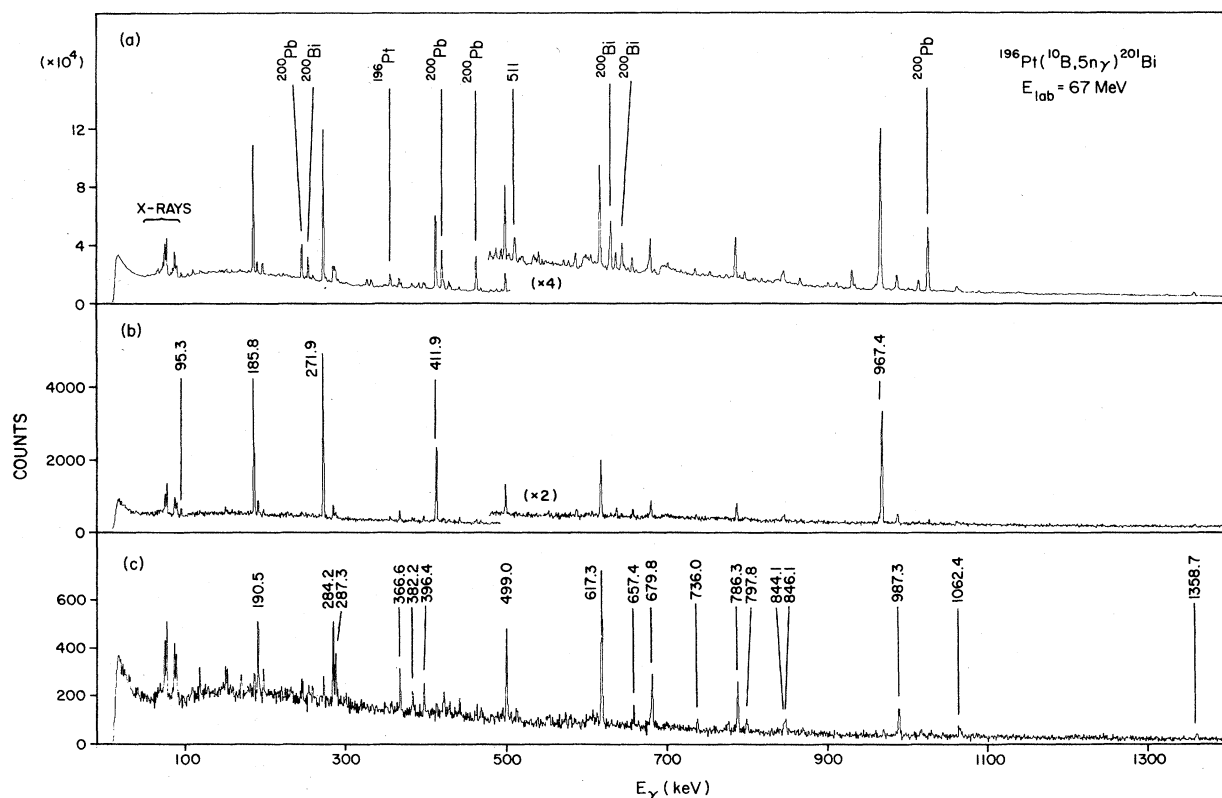

FIG. 2. (a) Spectrum of γ rays, produced by 67 MeV ^{10}B + ^{196}Pt, in coincidence with a second Ge(Li) detector. The most intense ^{200}Pb and ^{200}Bi transitions are labeled. (b) Summed spectrum of four ^{201}Bi background-subtracted γ-γ coincidence spectra gated on the 967.4, 411.9, 271.9, and 185.8 keV γ rays. (c) Same as (b) except that in addition a time-to-amplitude converter gating condition selects only those ^{201}Bi γ rays prior in time to the four transitions as discussed in the text.
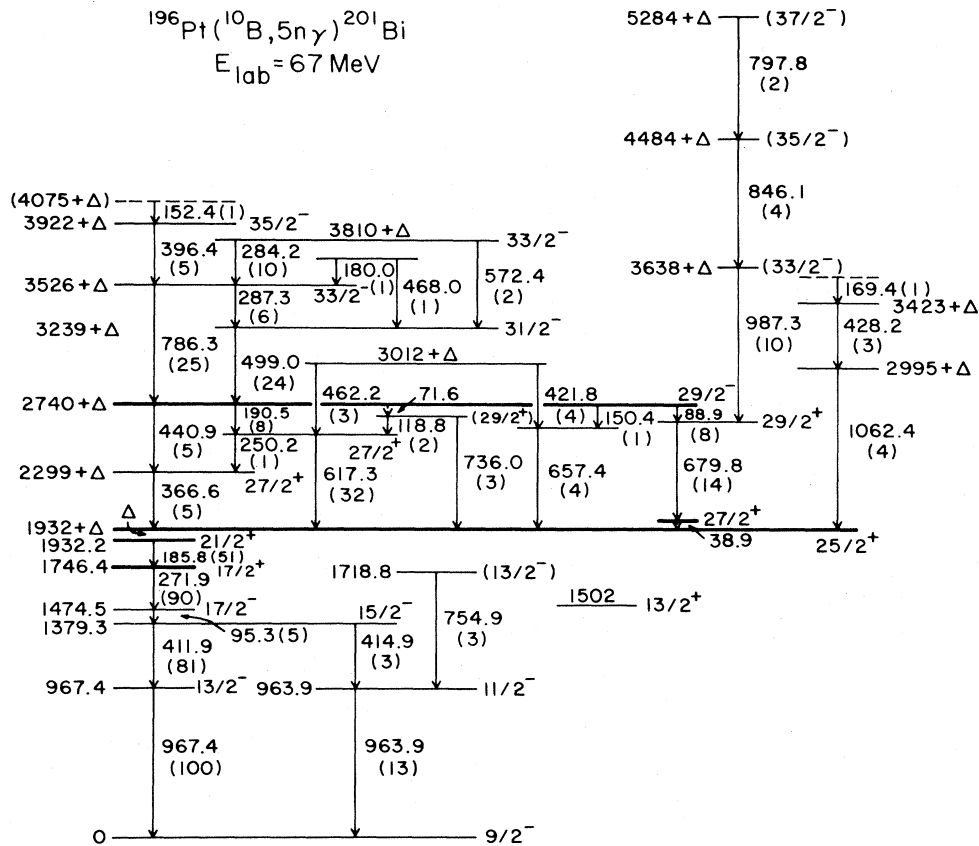
FIG. 3. Proposed level scheme for ^{201}Bi. The energies listed are in keV. The five isomeric levels are indicated by thick lines. Relative intensities, shown in parentheses, do not include internal conversion. The $\frac{13}{2}^{+}$ single-proton level shown was observed previously in ^{201}Po decay (Wood, private communication).

at $-90°$ and $154°$. The results were recorded event by event on magnetic tape for subsequent analysis. This detector geometry had the advantage that a partial γ-γ angular-correlation measurement was obtained, in addition to the coincident-intensity information. For a pair of coincident γ rays, γ_1 and γ_2, the correlation ratio R is defined as:

$$R = \frac{I[\gamma_1(-90°),\gamma_2(154°)]}{I[\gamma_1(154°),\gamma_2(-90°)]}, \qquad (1)$$

where $I[\gamma_1(-90°),\gamma_2(154°)]$ is the efficiency-corrected rate for detecting γ_1 in the $-90°$ detector in coincidence with γ_2 in the $154°$ detector. The ratio R was determined for several transitions, whose multipolarity was of interest, with known stretched $E2$ transitions in strong coincidence. The empirical ratios are compared with ratios calculated for various possible level spins and γ-ray multipolarities. This, together with extracted coincident intensities, provided a valuable consistency check and a test against contaminating γ rays.

The level schemes were constructed on the basis of the coincidence information, in combination with measured singles γ-ray intensities. Excitation functions, lifetime information, and conversion-coefficient limits extracted

from measured γ-ray intensities also aided in these assignments.

The decay rates of isomeric states were measured using ^{10}B beams pulsed with a repetition period of 2 μs and a pulse width of about 10 ns FWHM. Decay curves were extracted for the γ rays of interest, and the decay time $(t_{1/2})$ as well as the intensity of the delayed component were obtained from computer fits to time intervals starting after the pulse. For the pulsed-beam experiments, data were acquired using both a large Ge(Li) detector and an intrinsic Ge planar detector.

III. RESULTS

Excited states of ^{199,201}Bi had previously been studied out of beam[13,17,18] following the β^+-EC decay of the $\frac{3}{2}^-$ and $\frac{13}{2}^+$ isomers of ^{199,201}Po as mentioned. Figure 1 shows the observed γ-ray yields for ^{10}B + ^{196}Pt as a function of the ^{10}B beam laboratory energy for several of the ^{201}Bi(5n) transitions known from the previous studies. For comparison, the yields for the most intense transitions in the neighboring odd-odd ^{200}Bi(6n) and ^{202}Bi(4n) channels are also shown.
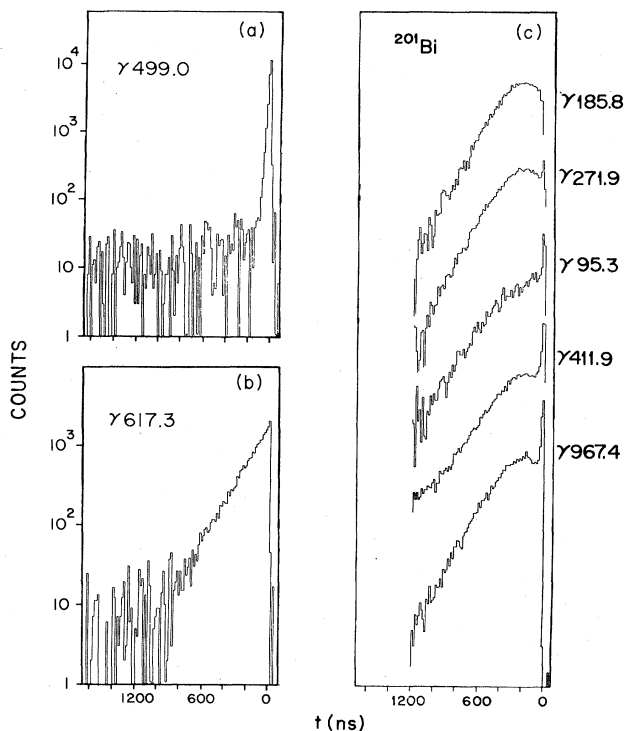
FIG. 4. (a) Distribution of time delays from the pulsed beam-γ measurements for the 499.0 keV transition in ^{201}Bi. (b) Similarly for the 617.3-keV transition in ^{201}Bi. (c) Similarly for five low-lying ^{201}Bi transitions. All of these time spectra (semi-log plots) were obtained with a large Ge(Li) detector except for the 95.3-keV spectrum, which was recorded using an intrinsic Ge planar detector. The relatively large prompt component shown for the 95.3 keV γ ray indicates that it lies below the 271.9- and 185.8-keV transitions as shown in Fig. 3.

A. Levels of ^{201}Bi

Figure 2(a) shows the open-gated γ-ray spectrum obtained from a ^{10}B + ^{196}Pt γ-γ-t coincidence experiment at 67 MeV. Displayed in Figs. 2(b) and (c) are the sum of four background-subtracted γ-ray spectra gated on the transitions: 967.4, 411.9, 271.9, and 185.8 keV. Figure 2(b) was obtained with no gating condition on the corresponding time-to-amplitude converter (TAC) signal, while for Fig. 2(c) only the prior time region of the TAC spectrum was included (0.5 μs range). Therefore, Fig. 2(c) implies the existence of isomeric delays (>5 ns) in ^{201}Bi. The background-subtracted spectra gated by individual transitions allowed the construction of the level scheme for ^{201}Bi as shown in Fig. 3 (see discussion below). The extracted γ-ray intensities, angular correlations, and angular-distribution information are listed in Table I. The relative intensities are, in general, obtained from singles measurements with good statistics, but are verified by the coincidence measurements; the latter are used where doublets prevented the resolution of a specific photopeak. When a γ ray, whose multipolarity is to be checked by γ-γ correlations, is coincident with more than one
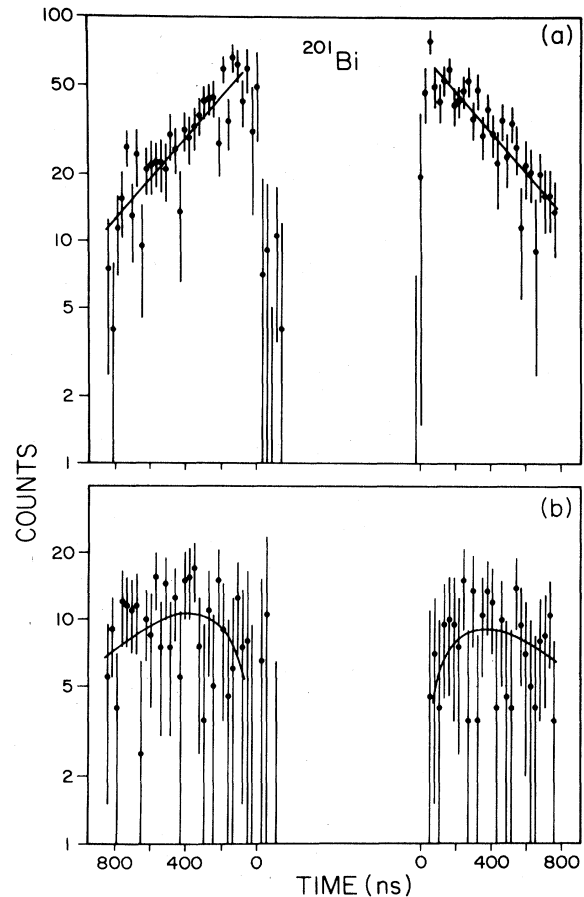
FIG. 5. (a) Distribution of time delays, obtained from γ-γ coincidence data, between the 617.3 keV γ ray in ^{201}Bi and the four transitions: 967.4, 411.9, 271.9, and 185.8 keV. These data are described well by a single lifetime, although a second short lifetime cannot be ruled out. (b) Distribution of time delays between the 679.8 keV γ ray in ^{201}Bi and the same four transitions. The fitted curve is a two-lifetime fit although a single-lifetime fit cannot be ruled out.

stretched $E2$ transition, the correlation ratios can be averaged in order to minimize the statistical uncertainty. For each correlation ratio listed in Table I, the number of stretched $E2$ transitions utilized is given in the sixth column.

Figure 4(c) summarizes the $\gamma(t)$ data for five low-lying ^{201}Bi transitions. It is seen that the 271.9 keV γ ray has relatively more intensity in the $t \approx 0$ peak than does the 185.8 keV transition, while the 95.3 keV γ ray, in turn, has even more. This is evidence that the ordering of these three transitions is as shown in Fig. 3, in agreement with the recent report by Broda *et al.*[20] An unobserved $\frac{25}{2}^+ \rightarrow \frac{21}{2}^+$ transition is placed in the level scheme, as shown in Fig. 3. The energy is less than 80 keV, otherwise it would have been observed. This transition is anticipated from the closeness of the yrast 7^- and 9^- ($\Delta E = 84$ keV) states in the ^{200}Pb core nuclide, while

TABLE I. Transitions in ^{201}Bi produced by the ^{196}Pt(^{10}B,5nγ)^{201}Bi reaction with $E_{\text{lab}}=67$ MeV. The A_2/A_0 and A_4/A_0 values have been corrected for the detector finite solid angle and the relative γ-ray intensities have been corrected for the Ge detector efficiency. The correlation R is defined by Eq. (1), while M is the number of coincident stretched $E2$ transitions used to determine R.

Transition energy (keV)	Relative γ-ray intensity	A_2/A_0	A_4/A_0	R	M	Assignment
38.9[a]						$\rightarrow \frac{25}{2}^+$
71.6[b]						$\frac{29}{2}^- \rightarrow (\frac{29}{2}_2^+)$
88.88±0.12	7.8±2.3[c]	d	d			$\frac{29}{2}^- \rightarrow \frac{29}{2}^+$
95.26±0.15	4.7±1.2	−0.04±0.18	−0.09±0.28	0.65±36	2	$\frac{17}{2}^- \rightarrow \frac{15}{2}^-$ Mostly $M1$
118.81±0.15	1.61±0.09	−0.08±0.12	+0.05±0.19			$(\frac{29}{2}_2^+) \rightarrow \frac{27}{2}_3^+$
150.45±0.60	0.92±0.06	−0.18±0.14	−0.18±0.22			$\frac{29}{2}^- \rightarrow$
152.36±0.35	1.46±0.15	−0.23±0.09	−0.07±0.15			$\rightarrow \frac{35}{2}^-$
169.40±0.35	0.61±0.07	−0.68±0.21	−0.02±0.33			$(\rightarrow 3423+\Delta)$
179.95±0.45	1.43±0.08	−0.13±0.11	+0.35±0.18			$\rightarrow \frac{33}{2}^-$
185.77±0.20	51.25±0.52	+0.157±0.010	−0.017±0.017	0.95±0.06	1	$\frac{21}{2}^+ \rightarrow \frac{17}{2}^+$
190.49±0.25	8.41±0.10	−0.128±0.024	−0.029±0.040			$\frac{29}{2}^- \rightarrow \frac{27}{2}_3^+$
192.5±0.7	3.7±0.7[c]	d	d			^{201}Bi
197.20±0.35	2.77±0.10	−0.05±0.08	−0.05±0.13			^{201}Bi
250.16±0.35	1.41±0.08	−0.24±0.11	+0.03±0.18			$\frac{27}{2}_3^+ \rightarrow \frac{27}{2}_2^+$ $1.5 \leq |\delta|^2$
258.37±0.35	2.33±0.08	−0.36±0.07	+0.04±0.11			^{201}Bi
271.91±0.20	89.98±0.90	+0.189±0.006	−0.012±0.009	0.922±0.044	1	$\frac{17}{2}^+ \rightarrow \frac{17}{2}^-$
284.19±0.25	10.01±0.22	+0.238±0.042	−0.098±0.070	0.67±0.27	1	$\frac{33}{2}_3^- \rightarrow \frac{33}{2}^-$ $|\delta| \leq 0.58$
287.29±0.35	6.4±0.9[c]	d	d			$\frac{33}{2}^- \rightarrow \frac{31}{2}^-$
366.62±0.35	4.6±0.8[c]	d	d	0.58±0.21	2	$\frac{27}{2}_2^+ \rightarrow \frac{25}{2}^+$
382.20±0.40	3.6±2.3[c]	d	d			^{201}Bi
396.44±0.35	5.18±0.08	−0.325±0.032	−0.010±0.053			$\frac{35}{2}^- \rightarrow \frac{33}{2}^-$ $\delta=-0.24±0.11$
411.86±0.20	80.7±2.2[c]	−0.128±0.004	−0.010±0.006	1.41±0.08	1	$\frac{15}{2}^- \rightarrow \frac{13}{2}^-$ $\delta=-0.023±0.017$
414.89±0.50	2.88±0.14	+0.07±0.06	+0.00±0.09			$\frac{15}{2}^- \rightarrow \frac{11}{2}^-$
421.84±0.50	4.3±0.7[c]	d	d			$2590+\Delta$
428.18±0.35	3.1±0.7[c]	d	d			$3423+\Delta \rightarrow 2995+\Delta$
440.87±0.35	5.11±0.12	−0.17±0.05	+0.12±0.08			$\frac{29}{2}^- \rightarrow \frac{27}{2}^+$
462.2±0.8	2.6±0.7[c]	d	d			$\rightarrow \frac{27}{2}_3^+$
467.96±0.40	1.4±0.7[c]	d	d			$\rightarrow \frac{31}{2}^-$
498.95±0.25	23.66±.24	−0.390±0.013	+0.032±0.022	1.14±0.22	2	$\frac{31}{2}^- \rightarrow \frac{29}{2}^-$ $\delta=-0.33±0.11$
552.49±0.35	1.16±0.12	−0.70±0.22	−0.40±0.34			^{201}Bi
572.45±0.40	1.96±0.17	−0.67±0.17	−0.23±0.27			$\frac{33}{2}_3^- \rightarrow \frac{31}{2}^-$ $\delta=-0.41±0.11$
617.27±0.25	32.31±0.33	−0.087±0.015	−0.015±0.023	1.02±0.10	2	$\frac{27}{2}_3^+ \rightarrow \frac{25}{2}^+$ $\delta=+0.046±0.028$
657.35±0.30	3.9±0.7[c]	d	d			$\rightarrow \frac{25}{2}^+$

TABLE I. (*Continued*).

Transition energy (keV)	Relative γ-ray intensity	A_2/A_0	A_4/A_0	R	M	Assignment
679.83±0.30	14.41±0.15	−0.312±0.015[e]	+0.020±0.025[e]	1.42±0.31	2	$\frac{29}{2}^+ \rightarrow \frac{27}{2}^+$ $\delta=-0.15\pm.12$
735.96±0.35	3.10±0.16	+0.20±0.11	−0.06±0.17			$(\frac{29}{2}^+{}_2) \rightarrow \frac{25}{2}^+$
754.89±0.35	2.60±0.12	−0.02±0.09	+0.60±0.15			$(\frac{13}{2}^-{}_2) \rightarrow \frac{11}{2}^-$
786.32±0.30	25.04±0.25	+0.113±0.014	+0.031±0.023			$\frac{33}{2}^- \rightarrow \frac{29}{2}^-$
797.85±0.40	2.26±0.11	+0.63±0.10	−0.07±0.16			$(\frac{37}{2}^-) \rightarrow (\frac{35}{2}^-{}_2)$
844.1±0.8	3.59±0.10	+0.05±0.06	−0.03±0.10			^{201}Bi
846.1±0.7	4.4±1.0[c]	+0.134±0.053[e]	+0.086±0.090[e]			$(\frac{35}{2}^-{}_2) \rightarrow (\frac{33}{2}^-{}_2)$
963.9±0.8	12.52±0.22	−0.152±0.035[e]	−0.023±0.057[e]			$\frac{11}{2}^- \rightarrow \frac{9}{2}^-$ $\delta=-0.04\pm0.07$
967.42±0.25	≡100.00±0.54	+0.152±0.011	−0.025±0.018			$\frac{13}{2}^- \rightarrow \frac{9}{2}^-$
987.31±0.35	9.97±0.14	+0.231±0.027	−0.056±0.046	0.75±0.40	2	$(\frac{33}{2}^-{}_2) \rightarrow \frac{29}{2}^+$
1062.4±0.8	4.34±0.15	+0.16±0.08	−0.01±0.11			$2995+\Delta \rightarrow \frac{25}{2}^+$
1358.71±0.45	3.26±0.11	+0.23±0.07	−0.18±0.12			^{201}Bi

[a]The evidence for this unobserved transition is based upon γ-γ coincidence relationships observed for preceding and following transitions.

[b]The evidence for this unobserved transition is based upon delayed lifetime data for the succeeding transitions

[c]The intensity is better determined from coincidence data.

[d]This transition is unresolved from another transition.

[e]This value may be perturbed by an unresolved transition.

TABLE II. Lifetime results for ^{199,200,201}Bi obtained both from γ-γ-t coincidence data (1 μs time range) and from pulsed beam-γ data (2 μs repetition period).

Nuclide	Level J^π, E (keV)	Present $t_{1/2}$ (ns)	Previous $t_{1/2}$ (ns)
^{201}Bi	$\frac{17}{2}^+$,1746.4	5.1±1.3	9.6±0.6[a]
	$\frac{21}{2}^+$,1932.2	<40	
	$\frac{25}{2}^+$,1932+Δ	118±28	210±20[a]
	$\frac{27}{2}^+$,1971+Δ	105±75	
	$\frac{29}{2}^-$,2740+Δ	124±4	160±30[a]
^{200}Bi	2241.8	37.4±1.6	46±4[b]
^{199}Bi	$\frac{17}{2}^+$,1647.5	34.1±2.4	
	$\frac{21}{2}^+$,1922.3	<50	
	$\frac{25}{2}^+$,1922+Δ	101±31	
	$\frac{29}{2}^-$,2523+Δ	168±13	

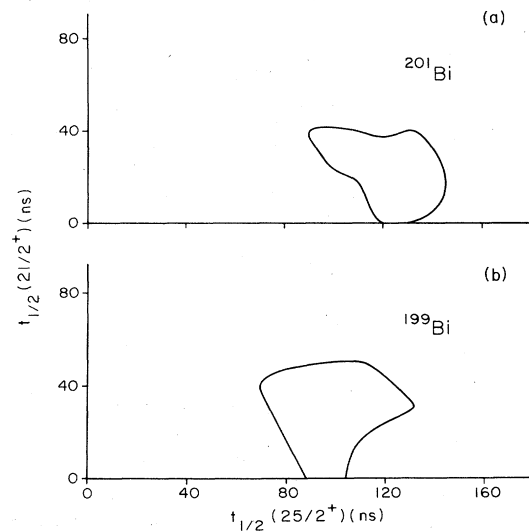[a]Reference 20.
[b]Reference 22.

FIG. 6. Results of the analysis of the ^{199,201}Bi lifetimes as discussed in the text. (a) The curve encloses the allowed ($\chi^2/\nu \le 1.5$) values for the half-lives of the $\frac{25}{2}^+$ and $\frac{21}{2}^+$ levels in ^{201}Bi obtained from the $\gamma(t)$ data for the 185.8 keV transition. (b) Similarly for the 274.8 keV transition in ^{199}Bi except that in this case $\chi^2/\nu \le 2.5$.
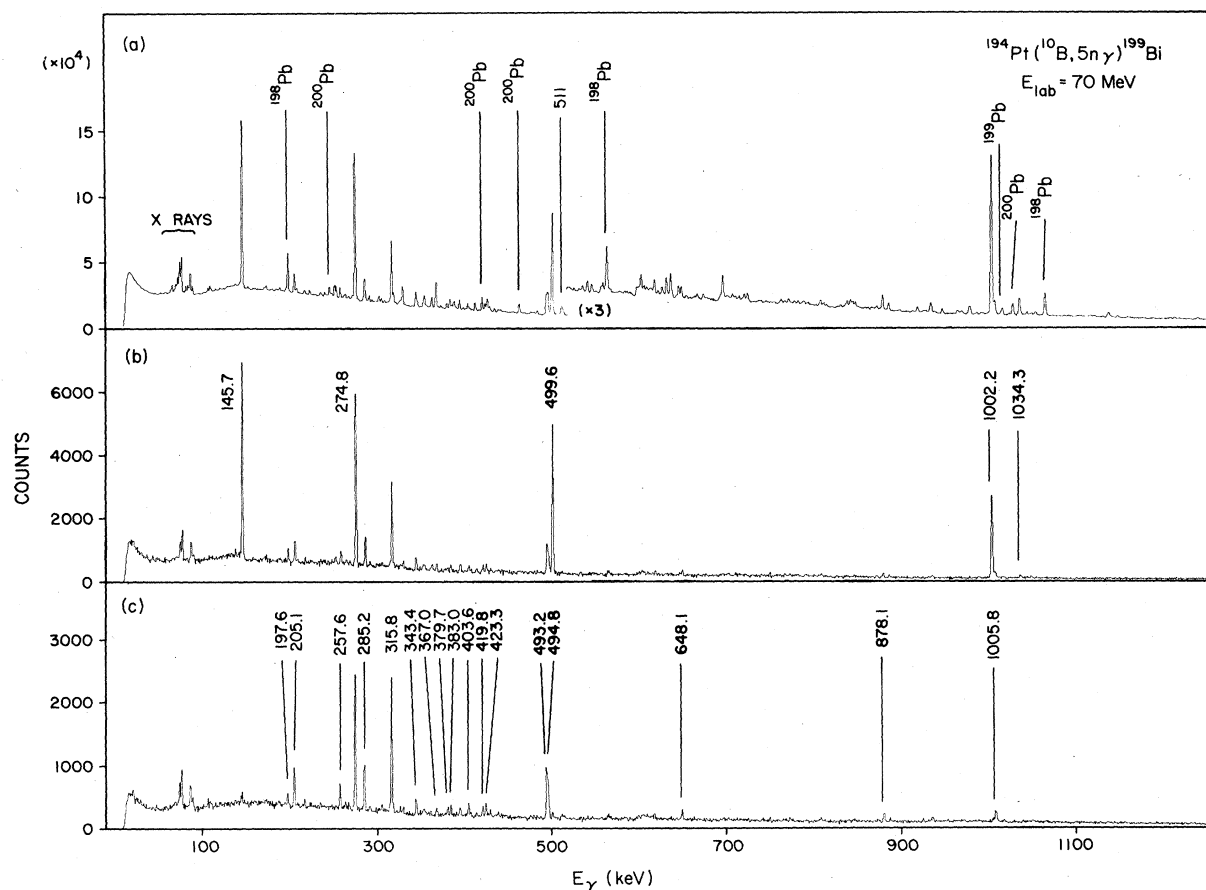
FIG. 7. (a) Spectrum of γ rays, produced by 70 MeV ^{10}B + ^{194}Pt, in coincidence with a second Ge(Li) detector. The most intense ^{198,199,200}Pb transitions are labeled. (b) Summed spectrum of four ^{199}Bi background-subtracted γ-γ coincidence spectra gated on the 1002.2, 499.6, 145.7, and 274.8 keV γ rays. (c) Same as (b) except that a TAC gating condition selects only those γ rays prior in time to the four transitions as discussed in the text.

analogous transitions have recently been reported in nearby ^{203,205}Bi by Hübel et al.[21] who observed the conversion electrons produced via the $(\alpha,4n\gamma)$ reaction. There are two additional unobserved transitions placed in the level scheme of Fig. 3. The existence of the 71.6-keV transition is indicated by the pulsed-beam data which show a delayed component of $t_{1/2} \sim 124$ ns both for the 118.8- and 736.0-keV transitions. The presence of the 38.9 keV transition follows since the 679.8 keV transition is observed in coincidence with the lower transitions with a time relationship shown in Fig. 5(b); further discussion is given below.

Five of the ^{201}Bi levels shown in Fig. 3 were found to be isomeric, i.e., $t_{1/2} \geq 5$ ns. The half-life of the $\frac{29}{2}^{-}$ isomeric level shown in Fig. 3 is best determined by the statistics of the 2 μs pulsed-beam $\gamma(t)$ data shown in Fig. 4(b) for the 617.3 keV transition. The result is $t_{1/2} = 124 \pm 4$ ns. An analysis of the $\gamma(t)$ data for the 499.0 keV transition

shown in Fig. 4(a) shows that an additional isomer with $t_{1/2} = 14 \pm 3$ ns occurs at or above the $3526 + \Delta$ keV level (the 786.3 keV γ ray also displays this delayed component). We are unable, however, to assign this half-life to a specific ^{201}Bi level. Broda et al.[20] have also found a half-life of ~ 10 ns from an isomer at or above the $3810 + \Delta$ keV level.

The other four isomers in ^{201}Bi were found from the γ-γ-t coincidence data. For example, Fig. 5 displays background-subtracted time-delay spectra associated with several γ-γ coincidences in ^{201}Bi. Figure 5(a) displays the sum of four time-delay spectra for the 617.3 keV transition in coincidence with each of the four transitions: 967.4, 411.9, 271.9, and 185.8 keV. Figure 5(b) shows the time-delay spectra for the 679.8 keV transition in coincidence with the same four transitions. The spectra in Fig. 5(a) are characteristic of a single intervening isomeric level, although the data do not rule out a short-lived

TABLE III. Transitions in ^{199}Bi produced by the ^{194}Pt(^{10}B,5nγ)^{199}Bi reaction with $E_{\text{lab}} = 70$ MeV. The A_2/A_0 and A_4/A_0 values have been corrected for the detector finite solid angle and the relative γ-ray intensities have been corrected for the Ge detector efficiency. The correlation R is defined by Eq. (1), while M is the number of coincident stretched $E2$ transitions used to determine R.

Transition energy (keV)	Relative γ-ray intensity	A_2/A_0	A_4/A_0	R	M	Assignment
80.0[a]						$\frac{29}{2}^- \to$
87.6[a]						$(\frac{29}{2}^- \to)$
107.31±0.40	1.5±1.1[b]	c	c			$\frac{27}{2}^+ \to \frac{25}{2}^+$
145.70±0.20	75.2±0.8	+0.133±0.004	−0.016±0.007	1.02±0.04	2	$\frac{17}{2}^+ \to \frac{17}{2}^-$
197.60±0.30	4.4±1.0[b]	c	c			$\to (\frac{27}{2}^-)$
205.13±0.25	7.68±0.09	−0.090±0.024	+0.034±0.039			$\to (\frac{27}{2}^-)$
239.76±0.40	1.81±0.10	+0.36±0.12	+0.03±0.19			$\to \frac{13}{2}^+$
251.13±0.25	6.40±0.07	+0.087±0.021	−0.064±0.035			$\frac{17}{2}^+ \to \frac{13}{2}^+$
257.55±0.25	4.80±0.08	−0.131±0.033	−0.029±0.054			$(\frac{27}{2}^-) \to \frac{25}{2}^+$
274.82±0.20	81.3±0.9	+0.130±0.004	−0.040±0.006	0.97±0.03	2	$\frac{21}{2}^+ \to \frac{17}{2}^+$
285.16±0.25	14.91±0.15	−0.185±0.012	+0.047±0.020	1.23±0.14	3	$\frac{29}{2}^- \to (\frac{27}{2}^-)$
315.80±0.20	38.86±0.39	−0.108±0.005	+0.044±0.009	1.25±0.13	3	$(\frac{27}{2}^-) \to \frac{25}{2}^+$
328.64±0.30	3.8±1.0[b]	c	c			^{199}Bi
343.41±0.30	5.5±0.9[b]	c	c			$(\frac{29}{2}^-) \to (\frac{27}{2}^-)$
352.05±0.35	2.86±0.06	−0.20±0.05	−0.20±0.08			$(\frac{19}{2}^-) \to \frac{17}{2}^+$
353.52±0.35	2.5±0.6[b]	c	c			$\to \frac{17}{2}^+$
362.01±0.25	6.13±0.11	−0.058±0.037	+0.084±0.061			$\frac{13}{2}^+ \to \frac{11}{2}^-$
366.96±0.25	5.2±1.1[b]	c	c			^{199}Bi
379.66±0.38	4.57±0.10	−0.38±0.05	−0.09±0.08			$(\frac{35}{2}^-) \to \frac{33}{2}^-$

second isomer as discussed below. By comparison, the spectra in Fig. 5(b) imply that more than one isomeric state occurs between the 679.8 keV transition and the 1932.2 keV level in ^{201}Bi. An analysis of these latter data yields a preliminary half-life for the $\frac{25}{2}^+$ level and 105±75 ns for the $\frac{27}{2}^+$ (1971 + Δ keV) level as listed in Table II. The extraction of the final value for the $\frac{25}{2}^+$ half-life is discussed below. The corresponding TAC spectra for the 185.8 keV transition in coincidence with lower-lying transitions appear to be nearly prompt. Further analysis, however, reveals a centroid shift leading to $t_{1/2} = 5.1 \pm 1.3$ ns for the $\frac{17}{2}^+$ isomer as listed in Table II. This value is somewhat shorter than the value of 9.6±0.6 ns reported by Broda *et al.*[20] The origin of the disagreement is unclear.

Figure 6(a) summarizes the results of computer fits to the pulsed-beam data for the 185.8 keV $\frac{21}{2}^+ \to \frac{17}{2}^+$ transition in ^{201}Bi where the aim is to constrain the possible half-lives of the $\frac{25}{2}^+$ and $\frac{21}{2}^+$ levels. Since the $\frac{25}{2}^+ \to \frac{21}{2}^+$ transition is unobserved, it is necessary to extract both half-lives simultaneously. The systematic behavior which has been found empirically for the analogous half-lives in ^{203,205}Bi indicates that the $\frac{25}{2}^+$ half-life should be longer than the $\frac{21}{2}^+$ half-life. Figure 6(a) displays the result of a four-lifetime fit where the half-

lives for the $\frac{27}{2}^+$ and $\frac{29}{2}^-$ levels are fixed at the values listed in Table II. The remaining two half-lives are allowed to vary while the relevant transition intensities are required to vary only within the bounds set by the experiment. The allowed region for the two half-lives lies inside of the solid curve, yielding the half-lives listed in Table II for the $\frac{21}{2}^+$ and $\frac{25}{2}^+$ levels. These values are in agreement with, and more definitive than, values obtained from the two-lifetime fit to the γ-γ-t coincidence data shown in Fig. 5(a). As seen in Fig. 6(a), the data do not distinguish between one- and two-lifetime fits; either case is possible.

The spins and parities shown in Fig. 3 are based on the angular distribution results given in Table I; the assignments of spin and parity in several cases are not unique but are considered to be the most probable. For several transitions, $E2/M1$ mixing ratios could be extracted; these are listed in the last column of Table I.

The ^{201}Bi level scheme resulting from the present study, which is shown in Fig. 3, is essentially in agreement with the recent results of Broda *et al.*[20] where overlap occurs; their level scheme contains 16 transitions while Fig. 3 contains 39 transitions, presumably because the present study is optimized for ^{201}Bi. It is useful, however, to point to several differences in the placement of transitions in the two level schemes. We see no evidence for levels at 2022 and 2272 keV as they have suggested. The 987.3

TABLE III. (Continued).

Transition energy (keV)	Relative γ-ray intensity	A_2/A_0	A_4/A_0	R	M	Assignment
383.05±0.25	8.48±0.15	−0.242±0.035	−0.111±0.057			$\frac{33}{2}^- \to \frac{31}{2}^-$
						$\delta = -0.10\pm0.11$
393.9	4.4±1.3ᵇ	c	c			[199]Bi
394.1	3.6±1.3ᵇ	c	c			$\frac{13}{2}^+ \to \frac{13}{2}^-$
403.65±0.25	2.58±0.13	+0.50±0.10	−0.10±0.16			$(2749 + \Delta \to)$
419.82±0.25	4.7±0.8ᵇ	c	c			[199]Bi
423.29±0.25	4.2±1.0ᵇ	c	c			$(\to \frac{25}{2}^+)$
493.17±0.30	18.94±0.19	−0.122±0.010	−0.003±0.006			$\frac{29}{2}^- \to \frac{27}{2}^+$
494.80±0.25	25.47±0.26	−0.390±0.008	+0.049±0.12			$\frac{31}{2}^- \to \frac{29}{2}^-$
						$\delta = -1.9\pm1.7$
499.61±0.20	85.4±0.9	+0.118±0.005	−0.039±0.007	1.01±0.05	1	$\frac{17}{2}^- \to \frac{13}{2}^-$
601.46±0.30	6.23±0.15	−0.086±0.048	−0.13±0.08			$\to \frac{11}{2}^-$
617.00±0.30	2.8±1.0ᵇ	c	c			$\to \frac{31}{2}^-$
617.22±0.40	≈2	c	c			$\to \frac{13}{2}^-$
648.09±0.25	6.44±0.11	−0.45±0.04	+0.00±0.06			$(\frac{27}{2}^+_2) \to \frac{25}{2}^+$
878.06±0.25	5.69±0.20	+0.38±0.08	−0.25±0.12			$\frac{33}{2}^- \to \frac{29}{2}^-$
885.02±0.30	4.84±0.13	−0.20±0.06	−0.07±0.09			$(\to \frac{31}{2}^-)$
933.60±0.35	4.12±0.13	+0.16±0.06	−0.02±0.10			[199]Bi
1002.19±0.20	≡100.0±0.3	+0.122±0.005	−0.010±0.008			$\frac{13}{2}^- \to \frac{9}{2}^-$
1005.82±0.30	8.62±0.13	+0.211±0.029	−0.124±0.049			$(\frac{29}{2}^-) \to \frac{25}{2}^+$
1034.31±0.30	17.86±0.18	−0.272±0.021	+0.045±0.034			$\frac{11}{2}^- \to \frac{9}{2}^-$
						$\delta = -1.3\pm1.0$

ᵃThe evidence for this unobserved transition is based upon γ-γ coincidence relationship observed for preceding and following transitions.

ᵇThe intensity is better determined from coincidence data.

ᶜThis transition is unresolved from another transition.

keV transition in their level scheme tentatively populated the $\frac{29}{2}^-$ level while we find it feeding a state 88.9 keV lower in energy. Figure 3 expresses our observation of prompt coincidences between the 679.8 and 88.9 keV transitions in disagreement with Broda et al. The present γ-ray angular distribution results are generally in agreement with those of Broda et al.[20] One exception seems worth mentioning—the 786.3 keV transition. They give −0.22±0.04 for A_2/A_0 while we find a value of +0.133±0.014 and assign this transition to be a stretched $E2$. In the present data, the singles and coincident intensities for this transition agree so that the angular distribution results are not strongly perturbed by any unresolved transitions. It is interesting to note that the alignment of nuclear spins achieved by the present ^{196}Pt(^{10}B,5nγ) study is less than was observed in the ^{203}Tl(α,6nγ) study.[20] For the three most intense γ rays which are stretched (185.8, 271.9, and 967.4 keV), we find an alignment coefficient $\alpha_2=0.37$ for (^{10}B,5nγ), while $\alpha_2=0.73$ describes the (α,6nγ) data; this presumably is the result of different hyperfine fields acting on the isomers.

B. Levels of ^{199}Bi

Figure 7(a) shows the open-gated γ-ray spectrum obtained from ^{10}B + ^{194}Pt at a laboratory energy of 70 MeV. Also shown in Figs. 7(b) and (c) are the sums of four γ-ray spectra gated on the transitions: 1002.2, 499.6, 145.7, and 274.8 keV. Figure 7(b) was obtained with no gating condition set on the TAC, while for Fig. 7(c), a delayed gating condition was set as was done for ^{201}Bi. Therefore, Fig. 7(c) implies the existence of isomeric delays in ^{199}Bi. The spectra gated by individual transitions led to the level scheme for ^{199}Bi as shown in Fig. 8. Information on the ^{199}Bi γ-ray transitions is summarized in Table III. The spins and parities shown in Fig. 8 are the most probable ones from a consideration of the γ-ray angular distribution results listed in Table III. For three transitions, values of the $E2/M1$ mixing ratio could be extracted, they are included in the last column of Table III.

Four of the levels displayed in Fig. 8 were found to be isomeric, i.e., $t_{1/2} \geq 5$ ns. Figure 9 displays background-subtracted time-delay spectra associated with γ-γ coin-

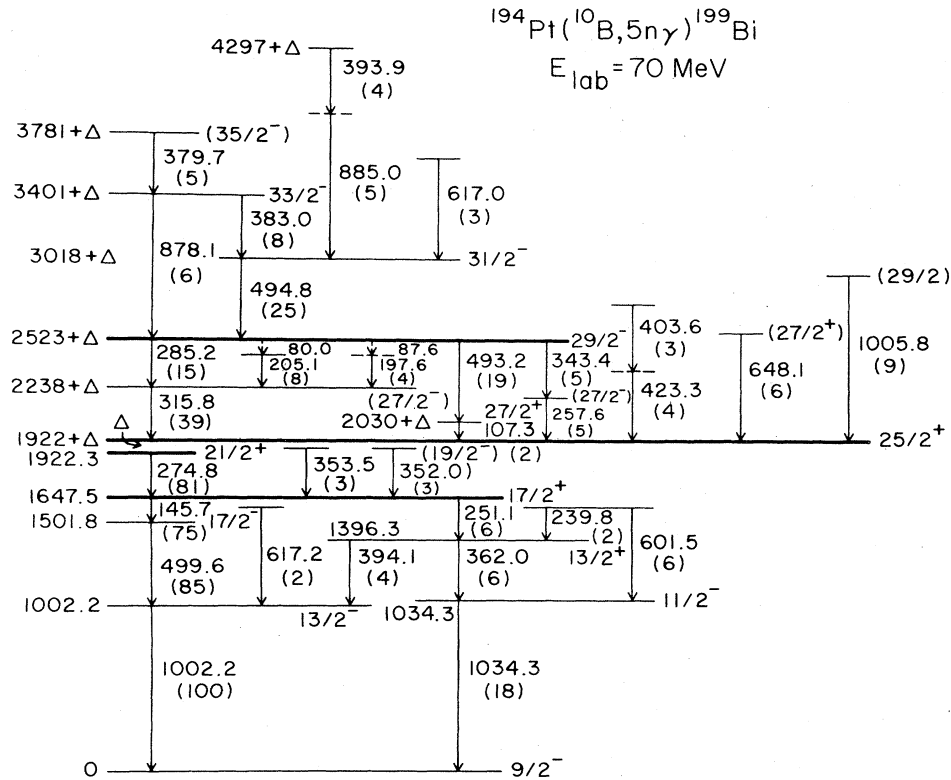$$^{194}Pt(^{10}B,5n\gamma)^{199}Bi$$

$$E_{lab} = 70 \text{ MeV}$$

FIG. 8. Proposed level scheme for ^{199}Bi. The energies listed are in keV. The four isomeric levels are indicated by thick lines. Relative intensities shown in parentheses do not include internal conversion.

cidences in ^{199}Bi. Figure 9(a) shows the time-delay spectra of the 274.8-keV transition in coincidence with the 145.7, 499.6, and 1002.2 keV transitions and Fig. 9(b) shows those for the 274.8-keV transition in coincidence with the 315.8-keV transition. The spectra in Fig. 9(a) indicate a single intervening isomeric level, while those in Fig. 9(b) suggest that two isomeric states occur between the 274.8- and 315.8-keV transitions, although the possibility of a single lifetime cannot be ruled out. The lifetime of the $\frac{29}{2}^{-}$ level shown in Fig. 8 was determined by the 2 μs pulsed-beam $\gamma(t)$ data for the 315.8 keV transition as shown in Fig. 10. As was the case for ^{201}Bi, the $\frac{25}{2}^{+} \rightarrow \frac{21}{2}^{+}$ transition of ^{199}Bi is unobserved in the present data. Thus, the half-lives of the $\frac{25}{2}^{+}$ and $\frac{21}{2}^{+}$ levels must be extracted simultaneously. To accomplish this, a three-lifetime fit was made to the pulsed-beam $\gamma(t)$ data for the 274.8 keV transition. The lifetime for the $\frac{29}{2}^{-}$ level was fixed at the measured value and the other two lifetimes were allowed to vary. During the fitting process, important constraints are provided by the relevant empirical transition intensities. The allowed values for the $\frac{25}{2}^{+}$ and $\frac{21}{2}^{+}$ half-lives are enclosed by the curve shown in Fig. 6(b), and the results are listed in Table III. Values can also be extracted for these two half-lives from the γ-γ-t coincidence data shown in Fig. 9(b). The results are less definitive but in agreement with those found from the $\gamma(t)$ singles data. As can be seen from Fig. 6(b), the data do not distinguish between a two-lifetime and a one-lifetime fit; either case is possible. There are two other unobserved

transitions depopulating the $\frac{29}{2}^{-}$ level which are implied on the basis of the γ-γ coincidence relationships: 80.0 and 87.6 keV.

C. Lifetime in ^{200}Bi

In the present lifetime measurements, delayed transitions, previously assigned to ^{200}Bi by Hagemann *et al.*,[22] were observed: 253.0, 286.1, 630.3, and 644.2 keV. The results are summarized in Table II where an average half-life of 37.4±1.6 ns is found. This is to be compared with the value of 46±4 ns reported by Kaun *et al.*[22]

IV. DISCUSSION

As pointed out in the Introduction, the first aim of this study in neutron deficient Bi isotopes is the examination of the systematic quasiparticle behavior of the odd-proton orbitals coupled to the neutron-hole states in the even-A Pb cores. This involves the identification of specific configurations and a determination of their excitation energies for theoretical comparisons. Further, since isomers and/or γ-ray branching ratios are observed, the corresponding electromagnetic transition rates can be extracted, which give information on the wave functions. The discussion below is divided into three subsections. Subsection A deals with details of the calculation of excitation energies for various configurations, in subsection B $E2$ and $E1$ transition rates are discussed, and subsection C is devoted to a comparison of the two odd-A chains of iso-
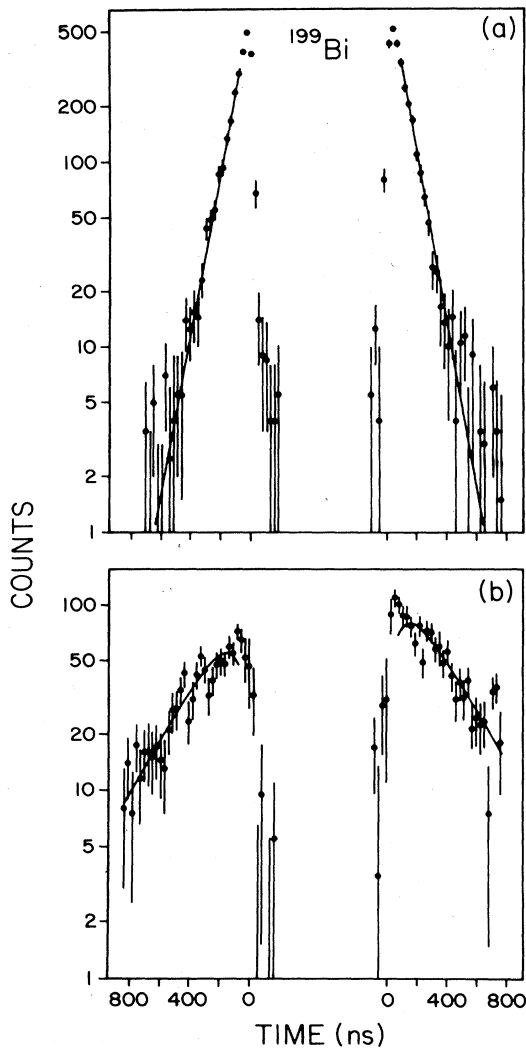
FIG. 9. (a) Distribution of time delays obtained from γ-γ coincidence data, between the 274.8 keV γ ray in ^{199}Bi and the three transitions: 145.7, 499.6, and 1002.2 keV. These data are described well by a single lifetime. (b) Distribution of time delays between the 274.8 and 315.8 keV γ rays. The curve is a two-lifetime fit as discussed in the text.

topes, Bi ($Z=83$) and At ($Z=85$). The second aim of this study involving collective aspects will be discussed in a subsequent paper.[16]

A. Excitation energies

The present experimental results relating to excitation energies in ^{199,201}Bi were given in Sec. III. In shell-model language, excited states in both nuclei can be described as consisting of a single proton coupled to ^{198}Pb and ^{200}Pb, respectively. The heavier Bi isotopes have been studied in great detail.[5—9] The yrast excitation energies in odd-A Bi are compared as a function of A in Fig. 11. It has been found that level energies calculated for specific shell-model configurations deviate increasingly from the experi-
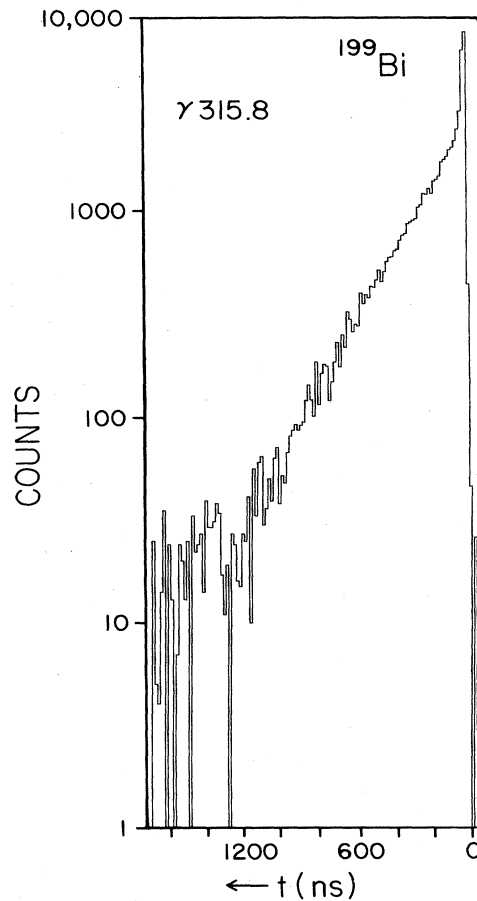

FIG. 10. Distribution of time delays for the 315.8-keV transition in ^{199}Bi obtained from the pulsed-beam measurements. The half-life derived from these data is listed in Table II.
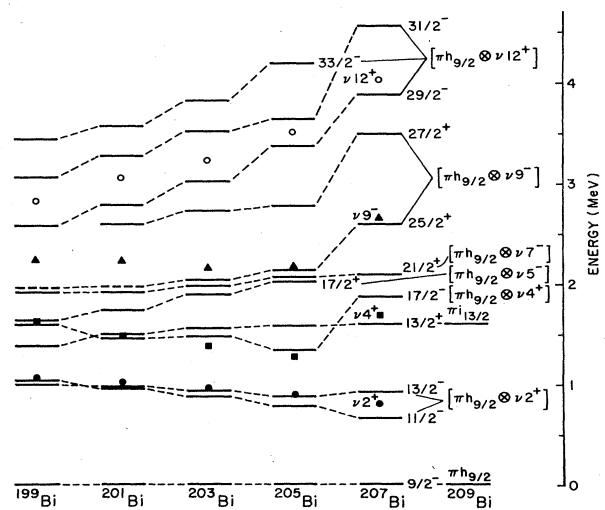

FIG. 11. Systematic comparison of three-quasiparticle and single-proton level energies in odd-mass Bi isotopes. The energies and J^{π} assignments for ^{203,205,207}Bi are from Refs. 5—9 and 21. Levels interpreted to have the main configurations listed on the right are connected by dashed lines.

mental energies as the number of valence nucleons increases. These increasing deviations are attributed to the complexity of the problem, i.e., to configuration mixing. In the present work, we have attempted to circumvent this problem of divergence by presenting a new method to calculate excitation energies that is nearly independent of the number of valence nucleons, as corroborated in the subsequent papers[15,16] dealing with ^{197}Bi and ^{195}Bi.

Many of the excited states in odd-A Bi isotopes can be described as a proton orbital ($\pi h_{9/2}$ is lowest in energy) coupled to the yrast 0^+, 2^+, 4^+ 5^-, 7^-, 9^-, and 12^+ states in the even-A Pb cores.[5-9] These core states are mainly of a two-quasiparticle nature. They involve the negative-parity $p_{1/2}$, $p_{3/2}$, $f_{5/2}$, and $f_{7/2}$ neutron-hole orbitals, and the unique-parity $i_{13/2}$ neutron-hole orbital. The excitation energies[14] of these neutron-hole orbitals are presented as a function of mass number A in Fig. 12. The 2^+ states involve predominantly $|vp_{1/2}^{-1}vf_{5/2}^{-1}\rangle$, and the 4^+ states are $|vf_{5/2}^{-1}vp_{3/2}^{-1}\rangle$ in ^{204}Pb and in the lighter isotopes.[5,23] The negative-parity core states involve the $vi_{13/2}^{-1}$ orbital coupled to the allowed low-lying negative parity orbitals. The 9^- states are relatively pure $|vf_{5/2}^{-1}vi_{13/2}^{-1}\rangle$. All three negative-parity states can also contain a nonyrast $|vf_{7/2}^{-1}vi_{13/2}^{-1}\rangle$ admixture, the amplitude of which should increase with decreasing mass number (Fig. 12). Finally, the 12^+ states should have a relatively pure $vi_{13/2}^{-2}$ configuration.

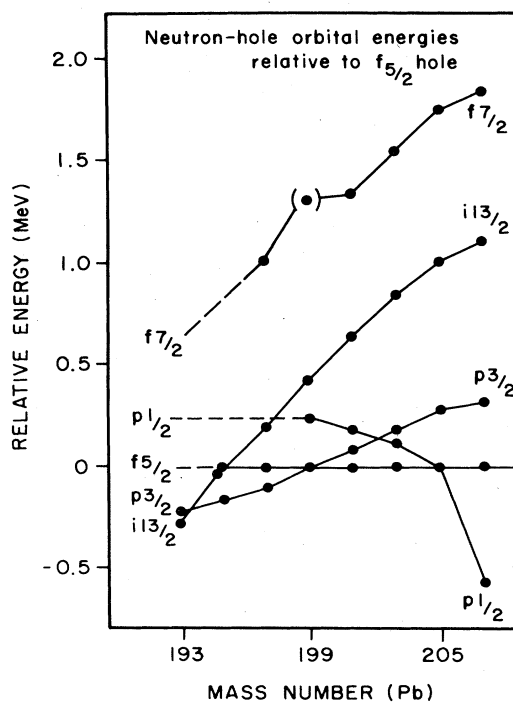Under the assumption that the lower-lying states in the

FIG. 12. Excitation energies of the neutron-hole orbitals in the Pb isotopes with $N < 126$ as a function of the mass number. The energy of the $f_{5/2}$ hole is set at zero for comparison.
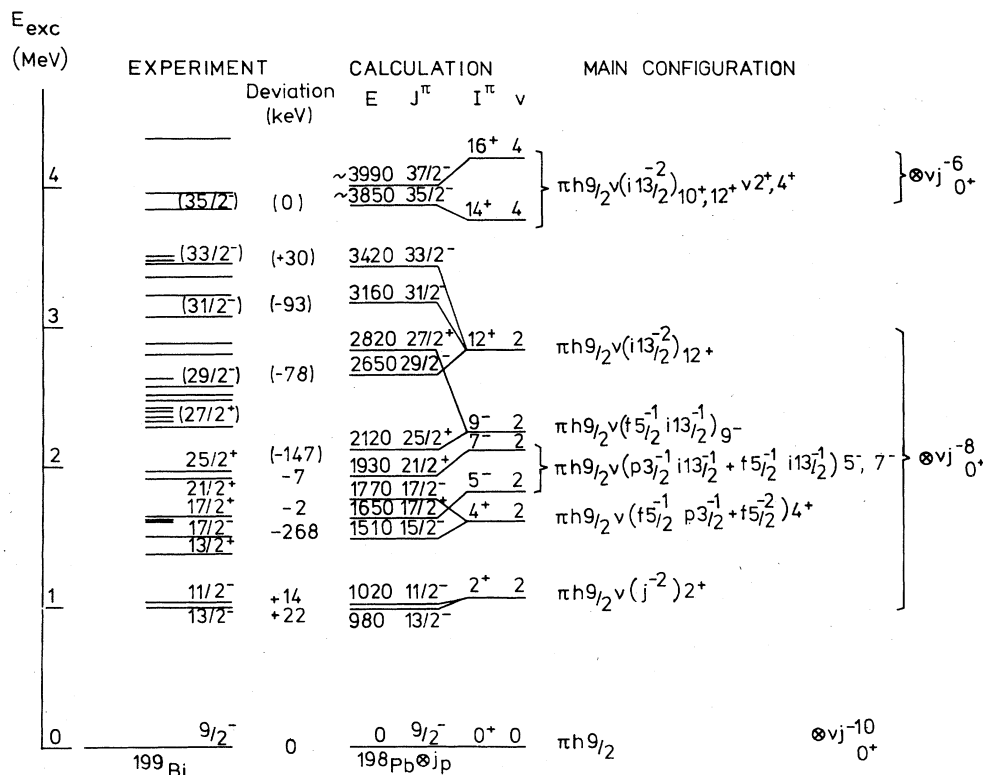

FIG. 13. Comparison of the calculated excitation energies with the experimental values for ^{199}Bi (see the text). The deviation is defined as $E_{exp} - E_{th}$.

TABLE IV. Relative interaction energies[a] (keV) of states in odd-A Bi isotopes.

I^π	J^π	$\Delta(I\otimes\pi h_{9/2};J)^{\text{b}}$	Neutron configuration
0^+	$\frac{9}{2}^-$	0 (Norm)	Mixed
2^+	$\frac{11}{2}^-$ $\frac{13}{2}^-$	$+90\uparrow$ $+30\downarrow$	Mixed
4^+	$\frac{15}{2}^-$ $\frac{17}{2}^-$	$+120$ $-95\uparrow$	$f_{5/2}^{-2}$ and $f_{5/2}^{-1}p_{3/2}^{-1}$
5^-	$\frac{17}{2}^+$	$+170$	$f_{5/2}^{-1}i_{13/2}^{-1}$ and $p_{3/2}^{-1}i_{13/2}^{-1}$
7^-	$\frac{21}{2}^+$	$+210$	
9^-	$\frac{25}{2}^+$ $\frac{27}{2}^+$	$+100\downarrow$ -550	$f_{5/2}^{-1}i_{13/2}^{-1}$
12^+	$\frac{29}{2}^-$ $\frac{31}{2}^-$ $\frac{33}{2}^-$	$+90$ -320 $-530\uparrow$	$i_{13/2}^{-2}$ $i_{13/2}^{-2}$
14^+	$\frac{35}{2}^-$	~ -100	$i_{13/2}^{-2}\otimes 2^+,4^+$
16^+	$\frac{37}{2}^-$	$\sim +200$	$i_{13/2}^{-2}\otimes 4^+$

[a]Extracted from states in ^{203,205}Bi (Refs. 5—8). See the text for details.

[b]The arrows indicate that Δ is not constant; a ± 50 keV slope adjustment is made in ^{199}Bi relative in ^{201}Bi.

odd-A Bi isotopes are of a three-quasiparticle nature, namely a single proton coupled to the two-quasiparticle Pb core states, their excitation energies can be calculated as follows. The states of the form

$$|J,^{A+1}\text{Bi}\rangle = |vI,^{A}\text{Pb}\rangle \otimes |j_\text{p}\rangle \; ,$$

where J is the spin of the state in the odd $^{A+1}$Bi nucleus, I the spin of the core state in the even Pb nucleus, and j_p refers to the odd proton. The states of this form are subsequently called a "three-body cluster." The energy of a state in $^{A+1}$Bi is given by the expression

$$E(J,^{A+1}\text{Bi})=E(I,^{A}\text{Pb})+E(j_\text{p})-\Delta(I\otimes j_\text{p};J) \; ,$$

where the $\Delta(I\otimes j_\text{p};J)$ is called the cluster interaction energy (in analogy with the conventional two-nucleon interaction energy). If the ground state is set at zero, the cluster interaction energy for $j_\text{p}=\pi h_{9/2}$, for which $E(j_\text{p})=0$, is obtained simply as

$$\Delta(I\otimes\pi h_{9/2};J)=E(I,^{A}\text{Pb})-E(J,^{A+1}\text{Bi}) \; .$$

The cluster interaction energies should be constant for constant core configurations and should vary smoothly for slowly changing configurations.

Table IV lists specific cluster interaction energies extracted from ^{203,205}Bi. Because of the strong influence of the $p_{1/2}$ neutron-hole orbital, ^{207}Bi was not used in the extraction. When the extracted interaction energies were not
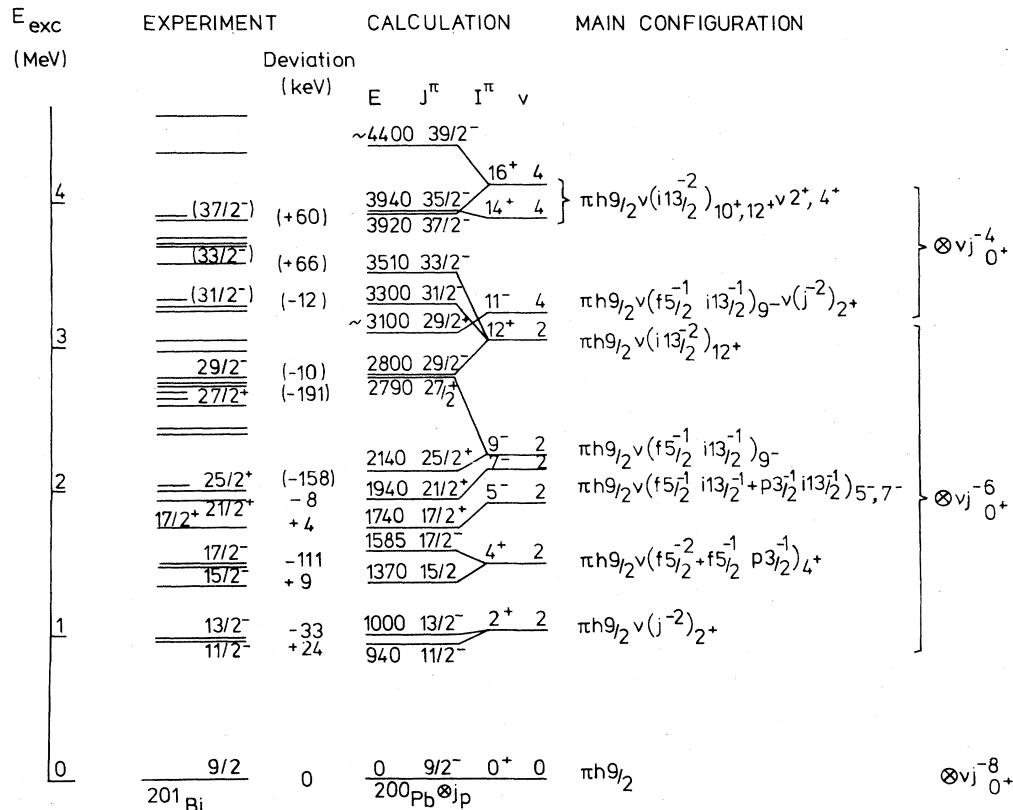

FIG. 14. Comparison of the calculated excitation energies with the experimental values for ^{201}Bi (see the text). The deviation is defined as $E_{\text{exp}}-E_{\text{th}}$.

perfectly constant, an additional energy-slope adjustment of ± 50 keV was made for [199]Bi relative to [201]Bi, as indicated by the arrows. These adjusted Δ values, as listed in Table IV, were then used in the energy expression above to obtain the values of $E(J,{}^{A+1}\text{Bi})$ for the three-quasiparticle states in [199,201]Bi. The calculated excitation energies are compared with the experimental values in Figs. 13 and 14.

The following general systematic trends of states from the present and previous[5–9,13,24] studies in [207–199]Bi are observed (see additional discussion including results of [197,195]Bi in the subsequent papers[15,16]).

1. Single-proton states

The single-proton states in the odd-Bi isotopes involve the odd-proton orbital j_p ($\pi h_{9/2}$, $\pi f_{7/2}$, or $\pi i_{13/2}$) coupled to the ground state $[E(0^+,{}^4\text{Pb})=0]$ for the Pb cores. The energy for the $\pi h_{9/2}$ ground states is defined as $E(j_p)=0$. The excitation energy $E(j_p)$ of the $\pi f_{7/2}$ orbital relative to the $\frac{9}{2}^-$ ground state, first increases by about 200 keV as the neutron number decreases from [209]Bi ($N=126$) and then stays almost constant down to [199]Bi.[24] The $\pi f_{7/2}$ state, being nonyrast, was not observed in the present measurements. In contrast, the energy of the $\pi i_{13/2}$ orbital remains practically constant down to [205]Bi and then decreases by about 200 keV in going to [199]Bi as shown in Fig. 11. This behavior can be understood on the basis of the average interaction energies of the πv^{-1} multiplets. The mean $\pi h_{9/2} v j^{-1}$ interaction (where j^{-1} stands for one of the neutron-hole orbitals of Fig. 12) is repulsive by about 200 keV, with the strongest repulsion taking place for the $\pi h_{9/2} v i_{13/2}^{-1}$ multiplet. For the $f_{7/2}$ proton, the mean repulsion is also about 200 keV, with the repulsion smallest in the $\pi f_{7/2} v p_{1/2}^{-1}$ doublet; this explains its energy increase near $N=126$, namely the repulsion is least when there are only a few neutron holes, which first populate the low-lying $v p_{1/2}^{-1}$ orbital. Finally, for the $\pi i_{13/2}$ proton, the repulsion is approximately constant at 190 keV for the lowest-lying neutron holes (Fig. 12), but decreases for the $v i_{13/2}$ hole; the net effect is a decrease in energy as N decreases. The relative energies $E(j_p)$ of the three proton orbitals as a function of N can thus be explained as arising from these differences in the πv^{-1} interactions as the various neutron orbitals in the core are successively depleted.

2. Three- (five-) quasiparticle states

The three-quasiparticle states in the odd-Bi isotopes are formed by coupling a proton orbital j_p to the predominantly two-quasineutron 2^+, 4^+, 5^-, 7^-, 9^-, and 12^+ states of the Pb cores. The states observed involve the lowest-lying proton orbital $\pi h_{9/2}$. The $\pi i_{13/2}$ proton orbital is not considered because of its relatively high excitation energy $E(j_p)\approx 1500$ keV, and the states involving the $\pi f_{7/2}$ orbital are nonyrast.

The three-quasiparticle states, which involve the odd proton particle coupled to a pair of neutron holes, are observed to follow the semiempirical $J_{\max}-1$ rule.[25] This rule predicts that the lowest energy member of a

$(v^{-2}I)\otimes(\pi j_p)J$ multiplet will have a spin $J=J_{\max}-1$. The reason for this behavior can be traced to the πv^{-1} particle-hole interaction energies. Aligned proton particle-neutron hole orbitals, which occur for $J=J_{\max}$ or $J_{\min}$, are most repulsive pushing these states up in energy. Other J members of the multiplet involving nonaligned orbitals are nearly degenerate at a lower energy; of these, the $J_{\max}-1$ state being yrast is most strongly populated.

The $(v^{-2}9^-)\otimes(\pi h_{9/2})J$ multiplet is a good example of this structure feature. The $J_{\max}-1=\frac{25}{2}^+$ members (see Fig. 11) are the lowest in energy at ≈ 2 MeV in [199,201]Bi and in [203,205]Bi (Refs. 7, 8, and 21) with the $J_{\max}=\frac{27}{2}^+$ pushed up in the energy range of 400–600 keV. For [207]Bi, the splitting is ≈ 900 keV.[6] A shell-model calculation of the relative energies of this multiplet can be made since the 9^- core states are of a rather pure $|\,v f_{5/2}^{-1} v i_{13/2}^{-1};9^-\rangle$ configuration. The results using empirical $v f_{5/2} \pi h_{9/2}$ and $v i_{13/2}^{-1} \pi h_{9/2}$ matrix elements[23] are shown in Fig. 15; the $J_{\max}-1=\frac{25}{2}^+$ state is lowest in energy with the $\frac{27}{2}^+$ pushed up by 840 keV. The strongly repulsive $\langle v i_{13/2}^{-1}\pi h_{9/2};11^-\,|\,V\,|\,v i_{13/2}^{-1}\pi h_{9/2};11^-\rangle$ aligned matrix element dominates the particle-hole interaction for the $\frac{27}{2}^+$ state. The nonaligned matrix elements are all of a weaker repulsive nature. This result, which is in agreement for the $\frac{27}{2}^+$-$\frac{25}{2}^+$ splitting in [207]Bi, is not in disagreement with the smaller experimental splitting in the lighter Bi isotopes because the $v^{-(n-2)}0^+$ components have been neglected (n is the number of neutron holes). In addition, the increasing $v f_{7/2}^{-1}$ admixture as N decreases can reduce the $\frac{27}{2}^+$-$\frac{25}{2}^+$ splitting since it allows a nonaligned component for the $\frac{27}{2}^+$ level. In fact, at least two $\frac{27}{2}^+$ levels were observed in both [199,201]Bi, making it difficult to determine the $J_{\max}=\frac{27}{2}^+$ member and its purity. The
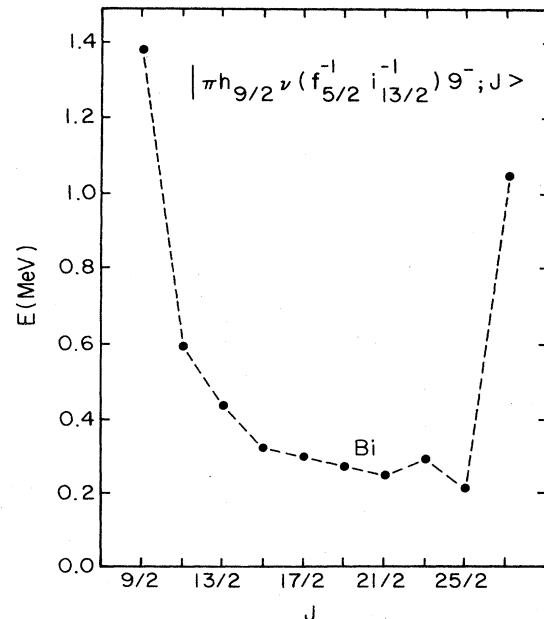

FIG. 15. Calculation of the relative energies of the $|\,\pi h_{9/2}(v f_{5/2}^{-1} v i_{13/2}^{-1})9^-;J\rangle$ multiplet as a function of J (see the text), which demonstrates the $J_{\max}-1$ rule (Ref. 25).

$J_{max}-1$ rule, which provides the explanation for the yrast nature of the $\frac{25}{2}^+$ member of the $\nu^{-2}9^-$ multiplet, also explains the yrast $\frac{21}{2}^+$ and $\frac{17}{2}^+$ levels as $J_{max}-1$ members of the $\nu^{-2}7^-$ and $\nu^{-2}5^-$ multiplets, respectively, as shown in Fig. 11.

The $J_{max}-1$ rule also appears to be valid for the $\pi h_{9/2}$ proton coupled to the more complicated $\nu^{-2}2^+$ core states in the heavier Bi isotopes. The $J_{max}-1=\frac{11}{2}^-$ level is lowest in energy with the $\frac{13}{2}^- - \frac{11}{2}^-$ splitting decreasing as N decreases and eventually reversing the order in ^{199}Bi (see Fig. 11). Configuration mixing smears out the $J_{max}-1$ effect as N decreases and eventually $J_{max}=\frac{13}{2}^-$ achieves the minimum energy as the neutrons of the core become more particlelike. The $\nu^{-2}4^+$ core multiplets show the $J_{max}-1=\frac{15}{2}^-$ state as the lowest energy member; however, in this case an inversion with $J_{max}=\frac{17}{2}^-$ was not observed.

For the $(\nu^{-2}12^+)\otimes(\pi h_{9/2})J$ multiplet, the observed yrast sequence is $\frac{29}{2}^- - \frac{31}{2}^- - \frac{33}{2}^-$ with the $J_{max}-2=\frac{29}{2}^-$ state lowest in energy. This sequence can also be understood microscopically from the $\pi\nu^{-1}$ interactions. Figure 16 summarizes the calculated results (filled circles) which are only in fair agreement with experiment. An admixture into the $\frac{29}{2}^-$ state from the $(\nu^2 10^+)$ core component (see open circle calculation in Fig. 16), which would depress its energy, is possible. No two-quasineutron configuration mixing occurs in the 12^+ core as a function of N, although four-quasineutron admixtures are possible. Detailed calculations regarding five-quasiparticle states are essentially impossible because of the many possible configurations. The $\nu^{-4}14^+$ and $\nu^{-4}16^+$ core states are required for $J\geq\frac{35}{2}^-$ states in ^{199,201}Bi and perhaps have some influence on other states, in particular, the $\frac{29}{2}^- - \frac{33}{2}^-$ level sequence.

3. Proton-hole states

In the heavier odd-A Bi isotopes, fairly low-lying $\frac{1}{2}^+$, $\frac{3}{2}^+$, and $\frac{5}{2}^+$ states have been observed.[13] They were ex-
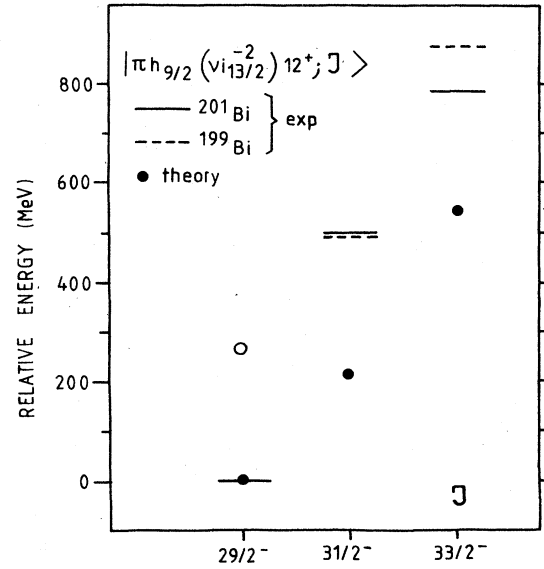

FIG. 16. Comparison of the calculated relative energies for the $|\pi h_{9/2}(\nu i_{13/2}^{-2})12^+;J\rangle$ multiplet (filled circles) with the experimental values for the $J^{\pi}=\frac{29}{2}^-$, $\frac{31}{2}^-$, $\frac{33}{2}^-$ sequence in ^{199,201}Bi. The $|\pi h_{9/2}(\nu i_{13/2}^{-2})10^+;\frac{29}{2}^-\rangle$ calculated energy is shown by an open circle.

plained as arising from proton-hole excitations of the $Z=82$ shell closure, and thus are attributed to the $s_{1/2}$, $d_{3/2}$, and $d_{5/2}$ proton-hole orbitals coupled to $(\pi j)^2 0^+$. Although these states are not observed in the present work, they have been seen in the β^+-EC decay of the corresponding odd-A Po isotopes.[24] Of interest for the present work, however, is the high-spin $h_{11/2}$ proton-hole orbital, which is expected to intrude to low energies via a prolate minimum in the potential energy surface, producing collective band structures.

Unfortunately the collective bands built on $h_{11/2}$

TABLE V. Transition probabilities of selected $E2$ transitions in Bi- and Pb-core nuclei with neutron numbers $N=116$, 118, 120, 122, and 124. The ^{199,201}Bi results are from the present experiment.

Nucleus transition		Transition probability (W.u.)					Dominant configuration
		$N=116$	118	120	122	124	
Bi		$A=199$	201	203	205	207	
	$\frac{17}{2}^+ \to \frac{13}{2}^+$	0.015					$\pi h_{9/2}\nu 5^- \to \pi i_{13/2}\nu 0^+$
	$\frac{21}{2}^+ \to \frac{17}{2}^+$	>0.09	>0.5	1.3	1.5		$\pi h_{9/2}\nu 7^- \to \pi h_{9/2}\nu 5^-$
	$\frac{25}{2}^+ \to \frac{21}{2}^+$	1.2–1.6[a]	1.0–1.4[a]	0.7	0.6		$\pi h_{9/2}\nu 9^- \to \pi h_{9/2}\nu 7^-$
Pb		$A=198$	200	202	204	206	
	$7^- \to 5^-$	>0.4	0.17	0.79			
	$9^- \to 7^-$	0.032–0.050[a]	0.26				
		0.17–2.20[b]					
	$12^+ \to 10^+$	0.62–0.83[a]	0.4–1.1[a]			0.33	

[a]Derived from the expression $(1+\alpha_{tot})E_{\gamma}^5$, assuming γ-ray energies between the L- and K-electron edges, namely $17 < E_{\gamma} < 88$ keV.

[b]Derived assuming γ-ray energies between the M- and L-electron edges, namely $4 < E_{\gamma} < 12$ keV.

proton-hole states were not observed. Using the energies of the lower spin proton-hole states, the estimated energy for the $\frac{11}{2}^-$ proton-hole state is about 1.8 MeV in ^{201}Bi and about 1.5 MeV in ^{199}Bi, as compared to 1 MeV for the lowest lying $\frac{11}{2}^- - \frac{13}{2}^-$ three-quasiparticle pair in both isotopes. The nonyrast character of the $h_{11/2}$ intruders thus makes them difficult to study. A possible explanation for their absence is a preference of the potential energy surface for an oblate minimum.[26] These collective aspects will be discussed in the subsequent paper on ^{195}Bi.[16]

B. Transition strengths

The question as to whether the Pb cores will start to develop stable collective effects as neutrons are removed has been of long-standing theoretical interest. Such collective effects would be manifest in, e.g., the excited-state properties of Bi and At isotopes.[1] Electromagnetic transition strengths obtained from measured lifetimes are very sensitive to collectivity.

In order to investigate the $E2$ electromagnetic matrix elements, the $E2$ transition probabilities extracted for the odd-A Bi isotopes are summarized in Table V. A suggested systematic trend as a function of N is the increase in the $\frac{25}{2}^+ \rightarrow \frac{21}{2}^+$ $E2$ strengths by a factor of about 2 in going from ^{205}Bi to ^{199}Bi. For ^{199,201}Bi, the $\frac{25}{2}^+ \rightarrow \frac{21}{2}^+$ $E2$ transition probabilities, however, could not be extracted precisely from the measured lifetimes because the γ-ray energies are unknown. Despite the fact that these γ rays were not observed, due to low energies and significant internal electron conversion, the transition energies are limited to $E_\gamma < 90$ keV by the knowledge of the experimental detector efficiency and the conversion coefficients as a function of energy. This upper limit to E_γ constrains the $E2$ transition probabilities to a fairly narrow range because of the near constancy of the expression $(1+\alpha)E_\gamma^5$ for energies between the L- and K-electron edges, namely $17 < E_\gamma < 88$ keV. As E_γ decreases, the total conversion coefficient α increases rapidly enough so as to partially balance the decrease in E_γ^5. The resulting transition-strength ranges for ^{199,201}Bi, as listed in Table V, still document the increase in the $\frac{25}{2}^+ \rightarrow \frac{21}{2}^+$ $E2$ strengths. The lifetime information for the $\frac{21}{2}^+$ states in ^{199,201}Bi is not sufficient to establish a similar trend for the $\frac{21}{2}^+ \rightarrow \frac{17}{2}^+$ $E2$ transition probabilities.

Since the $\frac{25}{2}^+ \rightarrow \frac{21}{2}^+$ Bi transitions are essentially a $9^- \rightarrow 7^-$ $E2$ transition of the Pb cores with the $\pi h_{9/2}$ proton as a spectator, it is interesting to examine the $E2$ strengths in the corresponding Pb-core nuclei for comparison. The available $E2$ transition probabilities for the Pb-core nuclei[27] are also listed in Table V. The $9^- \rightarrow 7^-$ $E2$ strength for ^{198}Pb shows an increase only if the unobserved γ ray had an energy between M- and L-electron edges, namely $4 < E_\gamma < 12$ keV. Such a small energy is consistent with the systematics. The $9^- \rightarrow 7^-$ $E2$ strength for an energy between the L- and K-electron edges is unreasonably small. These collective $E2$ enhancements for the Bi and Pb nuclei, if true, are consistent with small admixtures of the $\nu 2^+$ state assuming reasonable $2^+ \rightarrow 0^+$ $B(E2)$ strengths.[28] In contrast, the strength of the $12^+ \rightarrow 10^+$ $E2$ transition remains more constant; this can

be understood as resulting from the quenching that is related to the increased $\nu i_{13/2}$ neutron-hole population.[27] The lack of a large increase in the collectivity of the $\nu i_{13/2}^{-2}$ states between ^{206}Pb and ^{200}Pb is also seen in the quadrupole moments of the 12^+ states; the absolute value increases from about 0.5 fm^2 in ^{206}Pb to about 0.8 fm^2 in ^{200}Pb.[29] Since these values are not dependent on the structure of the 10^+ states as are the $B(E2)$ values, they provide a direct measure of the collectivity of the 12^+ states. The $\frac{17}{2}^+ \rightarrow \frac{13}{2}^+$ $E2$ transition in ^{199}Bi is hindered by a factor of about 70. This strong hindrance occurs because transitions between the dominant shell-model configurations $|\pi h_{9/2}, \nu 5^-; \frac{17}{2}^+\rangle \rightarrow |\pi i_{13/2}, \nu 0^+; \frac{13}{2}^+\rangle$ are forbidden. The measured $B(E2)$ is thus a direct measure of the admixed amplitude of the $|\pi i_{13/2}, \nu 2^+; \frac{17}{2}^+\rangle$ component in the initial state which has an allowed $E2$ transition.

The $E1$ transition strengths in the Pb region[14] are hindered by an average factor of about 5×10^6. The $E1$ transitions from the $\frac{13}{2}^+$ to the $\frac{11}{2}^-$ and $\frac{13}{2}^-$ states in ^{199,201}Bi were deduced to be relatively very fast. Because the lifetimes of the $\frac{13}{2}^+$ states were too short for direct measurement, the partial $E1$ lifetimes were calculated from measured branching ratios using the known $\frac{13}{2}^+ \rightarrow \frac{9}{2}^-$ $B(M2)$ value[1] for ^{201}At. These four $E1$ transitions are more than an order of magnitude faster than the average Pb-region value. A discussion of this $E1$ enhancement along with additional $E1$ results will be presented in the subsequent paper on ^{197}Bi.[15] The long $\frac{29}{2}^-$ isomeric lifetimes in the ^{199,201}Bi nuclei (see Table II) are a manifestation of the strongly hindered $\frac{29}{2}^- \rightarrow \frac{27}{2}^+$ $E1$ transitions.

C. Comparison of Bi and At yrast states

The observed properties of ^{199,201}Bi can be compared directly with the states involving seniority-one proton configurations in the isotonic ^{201,203}At ($Z=85$) nuclei.[1] The lowest states in these nuclides exhibit the same level sequence: $\frac{9}{2}^-$ (ground state), $\frac{11}{2}^-$, $\frac{13}{2}^-$, and $\frac{13}{2}^+$. The $\pi h_{9/2}$ and $\pi i_{13/2}$ proton orbitals, which couple to the 0^+ and 2^+ Pb cores to make these states in ^{199,201}Bi, are replaced by seniority-one $(\pi h_{9/2})^3$ and $(\pi h_{9/2})^2(\pi i_{13/2})$ configurations in ^{201,203}At. The ordering of the $\frac{11}{2}^-$ and $\frac{13}{2}^-$ states is reversed at neutron number $N=118$ (the ^{200}Pb core) in both Bi and At showing a consistent relaxation of the $J_{max} - 1$ rule[25] for the 2^+ core state. The $J_{max} - 1 = \frac{25}{2}^+$ state resulting from the 9^- Pb core state, however, is still lowest in ^{203}At as in ^{201}Bi, implying that the $J_{max} - 1$ rule is more applicable for the pure $|\nu f_{5/2}^{-1}, \nu i_{13/2}^{-1}; 9^-\rangle$ state. Calculations for the $\frac{27}{2}^+ - \frac{25}{2}^+$ splitting in At have been discussed previously.[3] In addition to these seniority-one proton states, the odd-A At isotopes[1–4] have yrast seniority-three proton states coupled to the 0^+ Pb cores. These include $(\pi h_{9/2})^3 \frac{21}{2}^-$, $(\pi h_{9/2})^2(\pi f_{7/2})\frac{23}{2}^-$, and $(\pi h_{9/2})^2(\pi i_{13/2})\frac{29}{2}^+$.

ACKNOWLEDGMENTS

*Present address: Physics Department, University of Pennsylvania, Philadelphia, PA 19104.

†Present address: Institute of Physics, University of Aarhus, DK-8000, Aarhus C, Denmark.

‡Permanent address: Physics Department, University of Jyväskylä, SF-40100, Jyväskylä, Finland.

§Permanent address: Atomic Energy of Canada Limited, Chalk River Nuclear Laboratories, Chalk River, Ontario, Canada K0J1P0.

[1]K. Dybdal, T. Chapuran, D. B. Fossan, W. F. Piel, D. Horn, and E. K. Warburton, Phys. Rev. C 28, 1171 (1983).

[2]T. P. Sjoreen, D. B. Fossan, U. Garg, A. Neskakis, A. R. Poletti, and E. K. Warburton, Phys. Rev. C 25, 889 (1982).

[3]T. P. Sjoreen, U. Garg, and D. B. Fossan, Phys. Rev. C 23, 272 (1981).

[4]T. P. Sjoreen, G. Schatz, S. K. Bhattacherjee, B. S. Brown, D. B. Fossan, and P. M. Lesser, Phys. Rev. C 14, 1023 (1976).

[5]T. Lönnroth, Z. Phys. A 307, 175 (1982).

[6]T. Lönnroth, J. Blomqvist, I. Bergström, and B. Fant, Phys. Scr. 19, 233 (1979).

[7]H. Hübel, A. Kleinrahm, C. Günther, D. Mertin, and R. Tischler, Nucl. Phys. A294, 177 (1978).

[8]R. Brock, C. Günther, H. Hübel, A. Kleinrahm, D. Mertin, P. Meyer, and R. Tischler, Nucl. Phys. A278, 45 (1977).

[9]T. Bergström C. J. Herrlander, P. Thieberger, and J. Blomqvist, Phys. Rev. 181, 1642 (1969).

[10]R. E. Shroy, A. K. Gaigalas, G. Schatz, and D. B. Fossan, Phys. Rev. C 19, 1324 (1979).

[11]R. E. Shroy, D. M. Gordon, M. Gai, and D. B. Fossan, Phys. Rev. C 26, 1089 (1982); 26, 1101 (1982).

[12]U. Garg, T. P. Sjoreen, and D. B. Fossan, Phys. Rev. C 19, 207; 19, 217 (1979).

[13]R. A. Braga, W. R. Western, J. L. Wood, R. W. Fink, R. Stone, C. R. Bingham, and L. L. Riedinger, Nucl. Phys. A349, 61 (1980).

[14]M. Pautrat, G. Albany, J. C. David, J. M. Lagrange, N. Poffe, C. Roulet, H. Sergolle, and J. Vanhorenbeeck, Nucl. Phys. A201, 449 (1973); A201, 469 (1973); C. Roulet, Ph.D. thesis,

Institut de Physique Nucléaire, Orsay, 1975; K. Honkanen, C. J. Herrlander, B. Fant, and T. Lönnroth, Nucl. Phys. A (to be published).

[15]T. Chapuran, D. B. Fossan, W. F. Piel, Jr., D. Horn, E. K. Warburton, T. Lönnroth, and K. Dybdal (unpublished).

[16]T. Lönnroth, D. Horn, E. K. Warburton, W. F. Piel, Jr., D. B. Fossan, K. Dybdal, and T. Chapuran (unpublished).

[17]A. Korman, D. Chlebowska, T. Kempisty, and S. Chojnacki, Acta Phys. Pol. 87, 141 (1976).

[18]M. Alpsten and G. Astner, Nucl. Phys. A134, 407 (1969).

[19]W. F. Piel, Jr., T. Chapuran, K. Dybdal, D. B. Fossan, D. Horn, and E. K. Warburton, Bull. Am. Phys. Soc. 26, 621 (1981); 27, 522 (1982); Proceedings on the 4th Nordic Meeting on Nuclear Physics, Fuglsø, Denmark, 1982, p. 34.

[20]R. Broda, C. Günther, and B. V. Thirumala Rao, Nucl. Phys. A389, 366 (1982).

[21]H. Hübel, M. Guttormsen, K. P. Blume, J. Recht, A. von Grumbkow, K. Hardt, P. Schüler, and Y. K. Agarwal, Z. Phys. A 314, 89 (1983).

[22]U. Hagemann, K. H. Kaun, W. Neubert, W. Schulze, and F. Stary, Nucl. Phys. A197, 111 (1972); Joint Institute of Nuclear Research Report E6-6808, Dubna, 1972.

[23]J. P. Schiffer and W. W. True, Rev. Mod. Phys. 48, 191 (1976).

[24]K. Heyde, P. van Isacker, M. Waroquier, J. L. Wood, and R. A. Meyer, Phys. Rep. 102, 291 (1983).

[25]L. Peker, Yad. Fiz. 1, 27 (1966), [Sov. J. Nucl. Phys. 4, 20 (1967)].

[26]P. Van Duppen, E. Coenen, K. Deneffe, M. Huyse, K. Heyde, and P. Van Isacker, Phys. Rev. Lett. 52, 1974 (1984).

[27]G. Albouy, G. Auger, J. M. Lagrange, M. Pautrat, H. Richel, C. Roulet, H. Sergolle, and J. Vanhorenbeeck, Nucl. Phys. A303, 521 (1978).

[28]I. Hamamoto, Phys. Rep. 10C, 63 (1974).

[29]H.-E. Mahnke, T. K. Alexander, H. R. Andrews, O. Häusser, P. Taras, D. Ward, E. Dafni, and G. D. Sprouse, Phys. Lett. 88D, 48 (1979).